Efficient Density Matrix Renormalization Group algorithm to study Y-Junctions with integer and half-integer spin

Manoranjan Kumar[1], Aslam Parvej[1], Simil Thomas[2], S. Ramasesha[3] and Z. G. Soos[4*]

[1] *S. N. Bose National Centre for Basic Sciences, Calcutta, Calcutta 700098, India*
[2] *Solar & Photovoltaics Engineering Research Center, King Abdullah University of Science and Technology, Thuwal 23955-6900, Kingdom of Saudi Arabia*
[3] *Solid State and Structural Chemistry Unit, Indian Institute of Science, Bangalore 560012, India*
[4] *Department of Chemistry, Princeton University, Princeton, New Jersey 08544, USA*

(Dated: August 14, 2015)

An efficient density matrix renormalization group (DMRG) algorithm is presented and applied to Y-junctions, systems with three arms of n sites that meet at a central site. The accuracy is comparable to DMRG of chains. As in chains, new sites are always bonded to the most recently added sites and the superblock Hamiltonian contains only new or once renormalized operators. Junctions of up to $N = 3n + 1 \approx 500$ sites are studied with antiferromagnetic (AF) Heisenberg exchange J between nearest-neighbor spins S or electron transfer t between nearest neighbors in half-filled Hubbard models. Exchange or electron transfer is exclusively between sites in two sublattices with $N_A \neq N_B$. The ground state (GS) and spin densities $\rho_r =< S^z_r >$ at site r are quite different for junctions with $S = 1/2$, 1, 3/2 and 2. The GS has finite total spin $S_G = 2S(S)$ for even (odd) N and for $M_G = S_G$ in the S_G spin manifold, $\rho_r > 0(< 0)$ at sites of the larger (smaller) sublattice. $S = 1/2$ junctions have delocalized states and decreasing spin densities with increasing N. $S = 1$ junctions have four localized $S_z = 1/2$ states at the end of each arm and centered on the junction, consistent with localized states in $S = 1$ chains with finite Haldane gap. The GS of $S = 3/2$ or 2 junctions of up to 500 spins is a spin density wave (SDW) with increased amplitude at the ends of arms or near the junction. Quantum fluctuations completely suppress AF order in $S = 1/2$ or 1 junctions, as well as in half-filled Hubbard junctions, but reduce rather than suppress AF order in $S = 3/2$ or 2 junctions.

PACS numbers: 75.10. Pq, 05.10.-a, 75.10.-b

I. INTRODUCTION

The transport and magnetic properties of a system with a junction of three wires have been a frontier area of research. Y junctions such as 3-terminal Josephson devices [1] or carbon nanotubes [2] have been studied experimentally. Understanding quantum effect in three terminal junctions is important for potential applications as rectifiers [2, 3], switches and logic gate devices [4]. Recently these systems have also been studied theoretically. [5–12] Interesting predictions include a low energy chiral fixed point with an asymmetric current flow in a spinless fermionic system [13] and negative density reflection at the junction of Bose liquid of ultra-cold atoms [14]. Theoretical studies have been mainly based on field theoretical approaches [14, 15].

Exact numerical results are limited to very small junctions and tend to be inconclusive, especially with respect to quantum many body effects. Numerical techniques such as density matrix renormalization group (DMRG) give excellent results for one-dimensional (1D) systems [16]. At first sight, however, DMRG appears to be far less accurate for structures with three terminals in which a long bond is repeatedly renormalized. Guo and White (GW) introduced [17] a new DMRG algorithm, summarized in Section II, for Y junctions with spin S at every site. We present in this paper a modified DMRG algorithm, quite distinct from that of GW, for Y-junctions with $N = 3n+1$ sites and three equal 1D arms of n sites. The accuracy and efficiency of the modified algorithm is comparable to DMRG in 1D chains, and we have studied Y junctions of up to 500 spins. We note that tensor-tree networks [18] are a general approach to many-body systems with a tree structure such as Y junctions, dendrimers or Bethe lattices. Stilbenoid dendrimers are a recent quantum chemical application [19] based on molecular units with many degrees of freedom. Tree networks based on different units call for diverse algorithms.

We consider Y junctions with antiferromagnetic Heisenberg exchange J between sites with spin S. The Hamiltonian for the junction in Fig. 1 is

$$H_S = J \sum_{\langle rr' \rangle} \mathbf{s}_r \cdot \mathbf{s}_{r'}. \quad (1)$$

The sum is restricted to adjacent sites and $J = 1$ is a convenient unit of energy. We discuss systems with $S = 1/2$, 1, 3/2 or 2 and also study fermionic junctions that correspond to half-filled Hubbard models with N electrons

* manoranjan.kumar@bose.res.in, aslam12@bose.res.in, simil.thomas@kaust.edu.sa, ramasesh@sscu.iisc.ernet.in, soos@princeton.edu

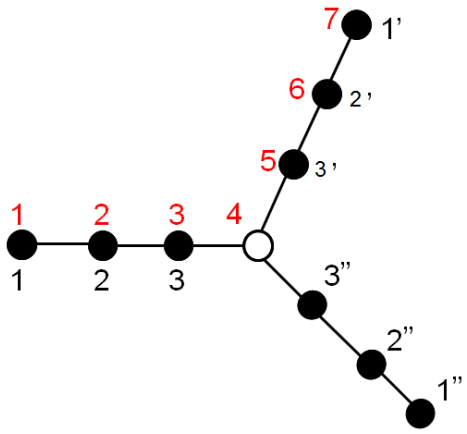

FIG. 1. Y junction of $N = 10$ sites with three equal arms of $n = 3$ sites. The numbering for the left (unprimed), up (primed) and down blocks (double primed) is used in the DMRG algorithm; the numbering in red is used for spin densities.

and N sites,

$$H_F = -t \sum_{\langle pp' \rangle \sigma} (a^+_{p\sigma} a_{p'\sigma} + a^+_{p'\sigma} a_{p\sigma}) + U \sum_p a^+_{p\alpha} a^+_{p\beta} a_{p\beta} a_{p\alpha}. \tag{2}$$

Electron transfer t (set to 1 to define the energy scale) is limited to adjacent sites p, p', the number operator is n_p, and $U > 0$ is repulsion for two electrons at a site. The Hückel or tight-binding limit of $U = 0$ is readily solved exactly and provides a direct check of accuracy. Trimethylenemethane, C_4H_6, is a Y junction with four π-electrons, four C atoms and has a stable triplet GS [20]. Bipartite Hückel models with many singly occupied π-orbitals are a design principle for high spin hydrocarbons [21]. The atomic limit $U >> t$ reduces H_F at half filling to H_S with $S = 1/2$ and $J = 4t^2/U$.

Both H_S and H_F conserve total spin S_T and its component S_z. By convention, we choose the Zeeman component $S_z = S_T$ when the ground state (GS) has spin $S_G > 0$. The spin density at site r is the GS expectation value

$$\rho_r = \langle S^z_r \rangle \tag{3}$$

The sum over sites r returns $S_z \geq 0$, but individual ρ_r may be positive or negative. Y junctions are bipartite: All exchange J or electron transfer t is between sites that form two sublattices, A and B, here with $N_A \neq N_B$ sites. The GS of H_S has $S_G = S|N_A - N_B|$, which alternates between $S_G = S$ and $2S$ for odd and even N, respectively. Sites in the larger sublattice have positive ρ_r, those in the smaller sublattice have negative ρ_r.

The paper is organized as follows. The modified algorithm for Y junctions with equal arms is presented and tested in Section II, including both infinite and finite DMRG algorithms. Its accuracy is fully comparable to DMRG for chains. As in chains, new sites are always bonded to the most recently added sites and the superblock Hamiltonian contains only new or once renormalized operators. The algorithm is applied to Y junctions in Section III, first to fermionic and $S = 1/2$ junctions, then to $S = 1$ junctions and finally to $S = 3/2$ and 2 junctions. We focus on spin densities and size dependence. Localized states in $S = 1$ junction are in excellent agreement with the valence bond solid (VBS) model of Affleck, Kennedy, Lieb and Tasaki (AKLT) [22]. There is a localized $S_z = 1/2$ state at the end of each arm and one centered on the junction. The localization length $\xi = 6.25$ in arms is close to the chain result of White and Huse [23] while the length $\xi_J < \xi$ indicates greater localization at the junction. The GS of $S = 3/2$ or 2 junctions up to 500 spins are unexpectedly different, however: They are spin density waves (SDWs) with increased amplitude at the ends of arms and near the junction. Antiferromagnetic (AF) order is possible in systems with $S_G > 0$ and found in Y junctions of $S > 1$ spins. Quantum fluctuations suppress AF completely in $S = 1/2$ or 1 junctions with long arms, but only partially in $S > 1$ junctions. We briefly mention in the Discussion generalizations of the algorithm to other junctions.

II. MODIFIED DMRG ALGORITHM

The computational effort for one eigenstate in conventional DMRG for 1D chains with open boundary conditions goes as $O(Nm^4)$ where N is the number of sites and m is the number of states per block for a given accuracy [24, 25]. The reason why is as follows: The number of arithmetic operations to obtain all eigenvalues of an $L \times L$ matrix is $O(L^3)$; so the number of operations for one eigenvalue goes as L^2. In DMRG the matrix size is $L = 16m^2$ for fermions and $L = (2S + 1)^2 m^2$ for spin S. In either case, L^2 goes as m^4 and a system of size N requires DMRG steps of $N/2$. This estimate excludes the construction and diagonalization of density matrices which are $O(m^3)$. The greatest cost is the superblock diagonalization that goes as $O(m^4)$ for one eigenstate.

Conventional DMRG for Y junctions scales as $O(m^6)$ and, as shown in Fig. 1c of ref. 17, involves a long bond whose operators are renormalized many times. GW [17] cite previous DMRG applications to Y junctions and present a more efficient scheme for junctions with three equal arms that meet at a point, as in Fig. 1, or at the vertices of an equilateral triangle. Singular value decomposition is used to obtain the density matrix of a single arm, and is faster as it requires $O(m^4)$ operations instead of $O(m^6)$. The method has a large truncation of the density matrix when two arms are combined

into a single block. We avoid truncation below since arms are never combined. The slow $O(m^6)$ step is the GS eigenvector of the superblock matrix, which goes as $L = O((2S+1)m^3)$ for three arms. The modified algorithm has improved accuracy for smaller m and makes it possible to treat Y junctions of $N \sim 500$ sites.

DMRG algorithms of 1D chains add two sites per step between the left and right blocks.[24, 25] The new sites are always bonded to the most recently added sites. The superblock Hamiltonian of chains only contains new operators or once renormalized operators, a desirable featured that we retain for Y junctions. In some algorithms the number of newly added site in the superblock can vary from one [26], two [17] or four [5] depending on the accuracy requirements of the systems. Here the superblock grows by three sites.

The modified algorithm is shown schematically in Fig. 2. Sites enclosed in loops define systems that consist of an arm plus a new site. The environment contains all sites in the other two arms. The key point is that the system at one step becomes an arm in the next step, thereby avoiding having to combine two arms into one block. The system block has $m \times r$ degrees of freedom, m for the arm and r for the new site, with $r = 4$ for fermionic junctions and $r = 2S+1$ for sites with spin S. The relevant dimension is not mr of the system block, however, because the density matrix is block diagonal in sectors with different M_S values. The time needed to diagonalize the density matrix is negligible in sectors of dimension $mr/(NS+1)$. We obtain all density matrix eigenvectors $|i\rangle$ of the system block by block diagonalizing it into different M_S sectors.

As shown in Fig. 2, we start with a superblock of four sites, $N = 3n+1 = 4$. The notation $(2,1,1)$ refers to an arm plus the central site and two other arms, respectively. The second step corresponds to $(3,2,2)$ and $N = 7$, the third to $(4,3,3)$ and $N = 10$, and so on. The $n+1$ sites of arm plus central site at step n become the arm at step $n+1$. We find the GS eigenvector $|\psi\rangle$ of the superblock, starting with $N = 4$, and expand $|\psi\rangle$ in the basis of the system (arm plus site) and the environment (two arms),

$$|\psi\rangle = \sum_{ik} C_{ik}|i\rangle|k\rangle. \tag{4}$$

The basis vectors $|k\rangle$ are direct products of basis states of two arms of the system of the previous step. The total number of sites, $N = 3n+1$, increases by three at each step. The reduced density matrix of the system has elements

$$\rho_{ij} = \sum_{k} C^*_{ik} C_{jk}. \tag{5}$$

The sum is over the environmental degrees of freedom. We suppose ρ to be a matrix of dimension M. After diagonalization, we take the m eigenvectors of ρ with the largest eigenvalues as elements of an $M \times m$ matrix ρ'. The effective Hamiltonian and operators in the truncated $m \times m$ basis are renormalized according to

$$\begin{aligned} O &= (\rho')^\dagger O \rho' \\ H &= (\rho')^\dagger H \rho' \end{aligned} \tag{6}$$

where $(\rho')^\dagger$ is the transpose matrix, and O and H are the operators and Hamiltonian of system block. The superblock eigenvalue calculation is the slow step that scales as $O(m^6)$, although conservation of total S_z reduces the dimension to less than $(2S+1)m^3$. The GS then yields the reduced density matrix ρ_{ij} of the system for the junction in which each arm is one site longer. Since operators of the system block are renormalized only once, similar to 1D chains, we expect similar truncation errors in Y junctions.

The following steps and Fig. 2 describe the infinite DMRG algorithm for Y junctions with equal arms:

(a) Start with four sites, the superblock in Fig. 2a.

(b) Find the GS eigenvalue and eigenvector.

(c) Construct the density matrix of the system block, shown in Figs 2a, 2b and 2c for 4,7 and 10 site superblocks, respectively. Diagonalize it to get the eigenvectors corresponding to the m largest eigenvalues.

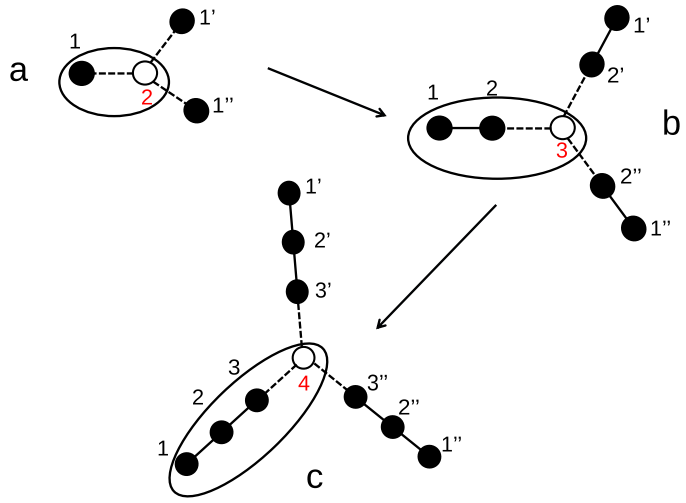

FIG. 2. Schematic representation of the infinite DMRG algorithm for Y junctions with equal arms. At each step, the loop encloses the system and the superblock contains a new site shown as an open dot, and three arms.

(d) Renormalize the operators and Hamiltonian for the system blocks using Eq. 6.

(e) Construct the Hamiltonian of the superblock as shown Fig. 2b and 2c.

(f) Repeat the process from b to e until the desired size $N = 3n + 1$ is reached.

Finite DMRG is required to obtain accurate spin densities, correlation functions and other GS properties. The conventional finite algorithm for 1D chains has two new sites and sweeps through two arms of the same chain [24, 25]. The algorithm for Y junctions has one new site and sweeps through two arms while keeping the third arm constant. The procedure is shown schematically in Fig. 3 and summarized below. Three to four DMRG sweeps are typically sufficient for converged energies. Finite DMRG is particularly important for junctions with $S = 3/2$ and 2 sites.

(a) Start with the superblock with equal arms as shown Fig. 3a taken from the infinite algorithm calculation. Select two arms A and B for sweeping through.

(b) Find the GS eigenvector of the superblock. The new system block 'A' is the old block A plus a new site, shown as the open dot in Fig. 3b. Block 'A' has one site added to arm A and removed from arm B at every step while arm C remains same. Construct the reduced density matrix of the system block 'A'.

(c) Renormalize the Hamiltonian and operators of the system block 'A'.

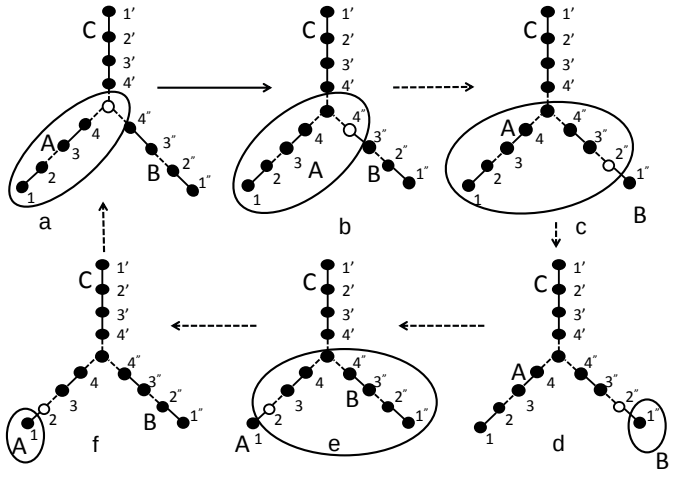

FIG. 3. Schematic representation of finite DMRG steps. Sites of the system block are enclosed in the loop; remaining sites are in the environmental block.The new site is the open dot. A, B and C arm refer to the three different arms.

TABLE I. The m dependence of the GS energy per site ε_0 of Y junctions with 64 sites, equal arms, and $U = 0$ in Eq. 2 or $S = 1/2$, $J = 1$ in Eq. 1.

m	$U = 0$	$S = 1/2$
20	-1.23336877828	-0.43915791387
40	-1.25809972580	-0.43915891861
60	-1.25826370430	-0.43915892503
80	-1.25838125000	-0.43915892523
100	-1.25842968750	-0.43915892525
Exact	-1.25848468281	-

(d) Construct the superblock Hamiltonian with new blocks 'A', 'B' and 'C' shown in Fig. 3b.

(e) Repeat the steps b to d until block 'B' has only one site as shown in Fig. 3c.

(f) Now take 'B' as the system block, block 'A' and 'C' as the environment. As shown in Fig. 3d, add a site to block 'B' and remove one from block 'A'.

(g) Repeat steps b to d for system block 'B' until block 'A' has only one site as shown in Fig. 3e.

(h) In the next step, 'A' becomes the system block. One site is added in 'A' and removed from block 'B'. Steps b to d are repeated until Fig. 3a is reached.

(i) Now take blocks 'A' and 'C' while keeping block 'B' constant and repeat the cycle a to h that starts and ends with equal arms in Fig. 3a. Finally, take block 'B' and 'C' while keeping the block 'A' constant. Repeat the cycle from a to h that starts and ends with Fig. 3a.

(j) One cycle of finite DMRG is the whole process from a to i.

Next we discuss the accuracy and efficiency of the algorithm. The $U = 0$ limit of Eq. 2 is a Hückel or tight-binding model of non-interacting electrons on N sites that can readily be solved exactly. As an example, we took a half-filled band of $N = 64$ sites and calculated the GS energy per site ε_0 as a function of m, the dimension of the system block in the truncated basis. Table I shows good convergence by $m \sim 60$ for this fermionic system of about 4^N degrees of freedom, or some 4^{21} per arm. DMRG of non-interacting electrons often converges the most slowly due to GS degeneracy or to higher entanglement entropy [26, 28]. The Y junction of $S = 1/2$ spins in Eq. 1 is the $U \gg t$ limit with 2^N spin degrees of freedom whose GS energy per site is not known exactly. As shown in Table I, $m \sim 20$ is sufficient for ε_0 of junctions with 21 spins per arm.

As additional tests of the algorithm, we consider the total energy $E(m)$ of 64-site Y junctions with $J = 1$ in

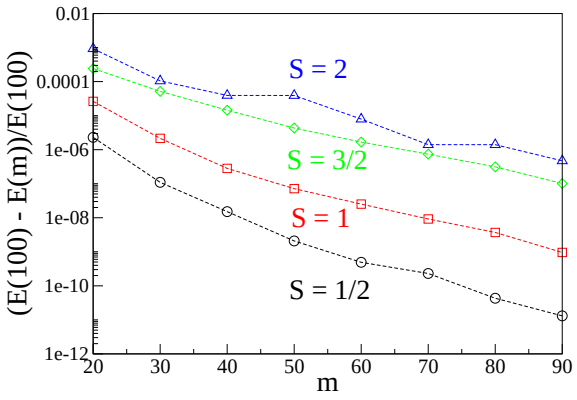

FIG. 4. Total GS energy $E(100)-E(m)$ as a function of m for 64-site Y junctions with equal arms, $J=1$, and the indicated S per site in Eq. 1.

Eq. 1 and $S = 1/2$, 1, 3/2 and 2 as a function of m. The truncation errors $P(m) = 1 - \sum_j^m \lambda_j$ on keeping m eigenvalues of the density matrix are listed in Table II for $S = 3/2$ and 2.

Since the exact GS is not known, we follow the evolution of $\Delta E(m) = E(m_0) - E(m)$ where $m_0 = 100$ is the nominally the converged value. Excellent convergence is achieved in Fig. 4 by $m \sim 70$, with ΔE of the order of 10^{-10} for $S = 1/2, 10^{-7}$ for $S = 1$, and 10^{-6} for $S = 3/2$ or 2. Increasing m to 130 lowers $\Delta E/E(100)$ by 5×10^{-7} for $S = 2$. The $P(m)$ change in Table II is also small. By contrast, the GW algorithm [17] for ΔE with $S = 1$ reaches only 10^{-6} around $m = 140$ in Fig. 3 of ref. 17. The present algorithm is well suited for Y junctions, both because as in 1D chains operators are renormalized only once and because the procedure in Fig. 2 increases the number of sites smoothly without ever having to combine two arms.

III. LOCALIZED STATES AND ANTIFERROMAGNETIC ORDER

We apply the modified DMRG algorithm to Y junctions with equal arms, either half-filled junctions in Eq. 2 or Heisenberg junctions with spin S at every site in Eq. 1. Unless otherwise stated, the results are based on $m = 100$ and $5-10$ sweeps of finite DMRG. We discuss junctions of $N = 3n+1$ sites, distinguish between odd and even N, and study the size dependence. The algorithm is applicable to junctions of $N \sim 500$ sites. We focus on AF order in Heisenberg junctions with $S > 1$ and on localized states of junctions with integer S.

TABLE II. Truncation errors $P(m)$ of 64-site Y junction of $S = 3/2$ and 2 as a function of m.

m	$P(m), S = 3/2$	$P(m), S = 2$
64	1.2×10^{-9}	7.2×10^{-6}
80	7.6×10^{-10}	3.0×10^{-6}
100	1.7×10^{-10}	1.5×10^{-6}
130	5.2×10^{-11}	5.6×10^{-7}

As mentioned in the Introduction, Y junctions are bipartite, with different number of sites $N_A \neq N_B$ in sublattices A and B. We take $N_A > N_B$ and have

$$N_A = \frac{N+1}{2} = N_B + 1 \quad (\text{odd } N, \text{even } n)$$
$$N_A = \frac{N}{2} + 1 = N_B + 2 \quad (\text{even } N, \text{odd } n). \tag{7}$$

The junction is in sublattice A for odd N, in sublattice B for even N. The Néel state $|AF\rangle$ has spins $\pm S$ at all sites in sublattices A and B, respectively, and is the SDW with the largest possible amplitude; $|AF\rangle$ is exact in the limit of classical spins, $S \to \infty$. Quantum fluctuations in Eq. 1 strongly reduce AF order for $S > 1$ and suppress it altogether for $S = 1/2$ or 1. Nevertheless, $|AF\rangle$ gives the correct spin, $S_G = 2S$ for even N and S for odd N, and also accounts for the sign of the GS spin densities in Eq. 3, with $\rho_r > 0$ for r in sublattice A and $\rho_r \leq 0$ for r in sublattice B.

A. Fermionic and $S = 1/2$ junctions

The Hückel junction has $U = 0$ in Eq. 2 and $N_A - N_B$ nonbonding orbitals with energy $\varepsilon = 0$ and nodes at all sites in sublattice B. The nonbonding orbitals are easily found analytically. The half-filled junction has N electrons, N sites and spin α in nonbonding orbitals. The GS for odd N has $S_G = 1/2$ and $\rho_r = 1/(2N_A)$ at sites in sublattice A, $\rho_r = 0$ at sites in sublattice B. The triplet GS for even N has $S_G = 1$, $\rho_r = 1/N_A$ at sites in N_A and $\rho_r = 0$ at sites in N_B. Since $S_G = 1$ for arbitrarily large (even) N, the Hückel densities at sites in sublattice A decrease as $2/(N+2)$.

Increasing $U > 0$ in the half-filled junction does not change S_G but induces negative $\rho_r < 0$ at N_B sites and increases $\rho_r > 0$ at N_A sites. The sum over $|\rho_r|$ increases with U as localized spins are formed due to electron correlations. The spin densities are no longer equal, however, as seen in Fig. 5 at $U = 4t$, the bandwidth of the 1D Hückel or tight-binding model. The Heisenberg model with $S = 1/2$ in Eq. 1 has the largest positive and negative spin densities.

The Heisenberg junction with even N has $\rho_J < 0$ at the junction and spin densities that go as $1/N$. The $S = 1/2$

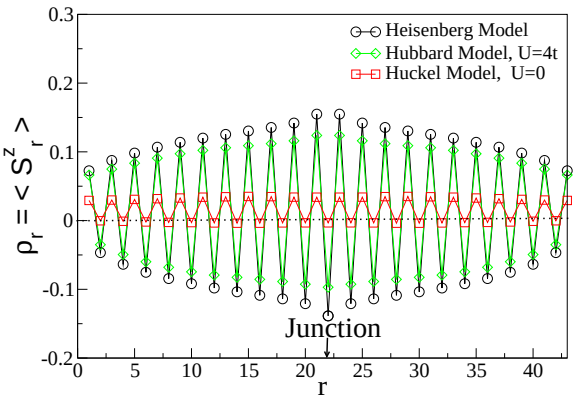

FIG. 5. Spin densities ρ_r along any two arms of 64-site Y junctions with $U = 0$ or $4t$ in Eq. 2, or $S = 1/2$ in Eq. 1. The junction is at $r = 22$ with $\rho_J \leq 0$.

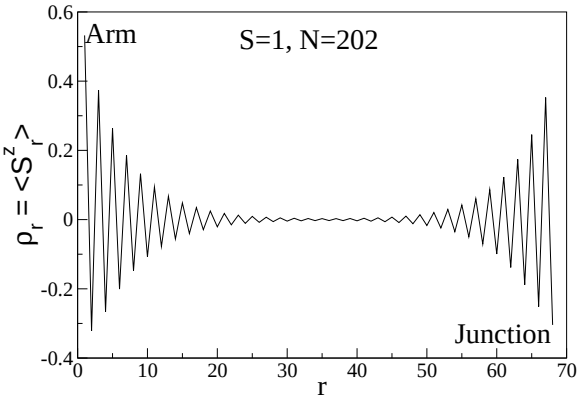

FIG. 6. Spin densities in one arm of a Y junction of $N = 202$ sites, $S = 1$, as a function of r with $r = 1$ at the first site and at $r = 68$ at the junction.

junction of $N = 202$ spins also has a triplet GS and a spin density distribution similar to the Heisenberg model in Fig. 5. Longer arms lead to smaller spin densities: $\rho_{68} = -0.0929$ for the junction at $r = 68$; $\rho_{67} = 0.0974$ and $\rho_{66} = -0.0817$ at the first and second neighbors of the junction; $\rho_1 = 0.0307$ and $\rho_2 = -0.0198$ at the first two sites of arms. As expected, quantum fluctuations entirely suppress AF order in the infinite $S = 1/2$ junction. We note that spin densities increase along the arms at odd r and become more negative at even r. We will later find a different pattern in $S = 3/2$ junctions in which quantum fluctuations are not as dominant.

B. $S = 1$ junctions

Haldane [29] predicted finite energy gaps $\Delta(S)$ in infinite Heisenberg spin chains with integer S and nearest neighbor $J > 0$. Experimental realizations of $S = 1$ chains have confirmed a gap that DMRG evaluates [23] as $\Delta(1)/J = 0.4105$. The valence bond solid (VBS) picture of AKLT [22] has been widely applied to $S = 1$ chains, and we do likewise for $S = 1$ junctions. $S = 1$ chains with open boundary conditions have a localized state with $S_z = 1/2$ and localization length $\xi = 6.03$ [23] at each end. GW [17] obtained four localized $S_z = 1/2$ states in a Y junction with $N = 181$, one at the end of each arm and one centered on the junction.

Figure 6 shows the spin densities in one arm of a Y junction of $N = 202$ sites with $S = 1$. As expected, the GS has $S_G = 2$, the junction at $r = 68$ has $\rho_J < 0$, and the total S_z of either localized state is $1/2$. The spin densities in the first 15 sites of an arm and 14 sites from the junction are listed in Table III. The spin densities of localized states are conventionally taken as proportional to [23, 30]

$$\rho_r \propto (-1)^{r-1} exp(-r/\xi) \tag{8}$$

where $r = 1$ refers to the ends of chains. This approximation neglects the difference between ρ_r for even and odd r that is clearly seen in Fig. 6 and Table III. Any pair r, $r + 2$ defines a local localization length [30] $\xi = 2/(ln|\rho_r| - ln|\rho_{r+2}|)$. As seen in Fig. 7, the $\rho_r > 0$ and $\rho_r < 0$ series have similar localization whose average is $\xi = 6.25$ for arms, $\xi_J = 5.81$ for the junction, and the first few sites deviate from a simple exponential. White and Huse [23] obtained $\xi = 6.03$ for $S = 1$ chains with open boundary conditions; they did not consider positive and negative spin densities separately. GW [17] report similar localization at the junction and arms without going into detail, while we find slightly but distinctly smaller $\xi_J = 5.81$.

We consider next Y junctions of $S = 1$ spins and odd $N = 199$. The GS is a triplet, $S_G = S_z = 1$, and the junction has $\rho_J > 0$. Quite remarkably, the spin densities of the localized state are identical to a part per 10^4 to the $N = 202$ values in Table III aside from a reversed sign around the junction. The localization lengths $\xi_A = 6.25$ and $\xi_J = 5.81$ obtained for $N = 202$ are equally applicable to $N = 199$ within our numerical accuracy. Spin densities near the junction add to three localized states at the ends of arms for $N = 202$ and $S_z = 2$, while they subtracts for $N = 199$ and $S_z = 1$. Identical $|\rho_r|$ for $N = 199$ and 202 directly confirm that each localized state has $S_z = 1/2$. The GS of a Y junction of $S = 1$ spins and long arms is $2^4 = 16$-fold degenerate and comprises a quintet, three triplets and two singlets. The quintet has A symmetry under C_3, the singlets transform as E, and the triplets as A and E.

TABLE III. Spin densities of a Y junction of $N = 202$ sites with $S = 1$. Listed are the first 15 sites of an arm, the junction and up to 14 sites from the junction.

spindensityρ_r	Arm, $r = 1$	Junction
1	0.5321	-0.3044
2	-0.3209	0.3530
3	0.3733	-0.2515
4	-0.2652	0.2459
5	0.2624	-0.1886
6	-0.2000	0.1737
7	0.1855	-0.1383
8	-0.1469	0.1234
9	0.1317	-0.1004
10	-0.1068	0.0880
11	0.0939	-0.0726
12	-0.0773	0.0629
13	0.0671	-0.0629
14	-0.0558	0.0450
15	0.0480	-0.0377

C. Junctions with $S > 1$

The Haldane gap of the infinite spin-2 chain is smaller, [31] $\Delta(2) = 0.0886 \pm 0.0018$, about $\Delta(1)/5$ and is less accurately known than $\Delta(1)$. The ends of $S = 2$ chains are expected to have localized $S = 1$ states with correspondingly larger ξ. Schollwöck *et al.* [30] have discussed the $S = 2$ chain in detail using DMRG, quantum Monte Carlo and exact diagonalization methods; they interpret results in a VBS framework and report [30, 32] limited agreement. Chains of $N = 270$ spins with increasing m (to 180) cover a 25-fold spin density change. Fig. 6 of ref. 28 shows $\xi = 2/(ln|\rho_r| - ln|\rho_{r+2}|)$ to vary as $\sim 40 \pm 10$ up to $r \sim 30$ and to be almost constant, $\xi \sim 50$, in the range $40 < r < 125$.

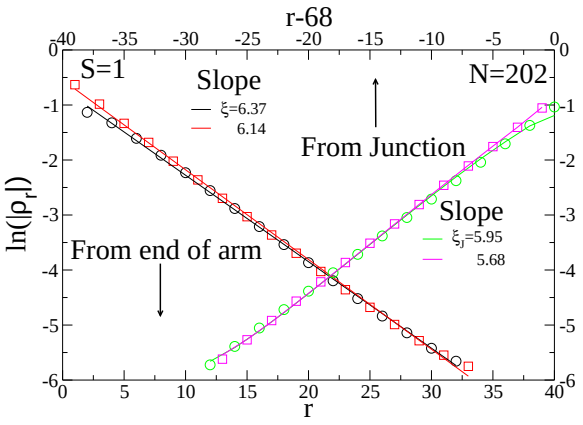

FIG. 7. Spin densities from Fig. 6 plotted as $ln|\rho_r|$ vs. r at an arm and at the junction. Circles (squares) represent negative (positive) spin density.

Smaller $\Delta(2)$ and localization $\xi \sim 50$ in $S = 2$ chains indicate that Y junctions with longer arms are needed to study localized $S = 1$ states. Instead of localized states, however, and in sharp contrast to $S = 1/2$ or 1 junctions, we find substantial AF order in both $S = 2$ and $S = 3/2$ junctions as shown in Fig. 8 for $N = 448$ (left panel) and 298 (right panel). The junction is at $r = 150$ or 100, respectively. The spin density in the interior of arms oscillates between $\pm c$ at odd and even r. The amplitude increases at the junction and at the end of arms, in contrast to the spin densities of the $S = 1/2$ junction in Fig. 5 whose magnitude decreases from the junction. The similarity in the behavior of the $S = 3/2$ and $S = 2$ junctions is noteworthy since the infinite $S = 3/2$ chain is gapless unlike the $S = 2$ chain. We consider the main features together before pointing out differences between $S = 3/2$ and 2 junctions.

By definition, Heisenberg exchange is between localized spins S at every site. The sum over ρ_r is the z component of spin in the given state. The sum over $|\rho_r|$ normalized to NS is the fraction of unpaired spins; the Néel state $|AF\rangle$ with $\pm S$ returns $(NS)^{-1}\sum_r |\rho_r| = 1$. We interpret SDW amplitudes c in Fig. 8 in the interior of arms as AF order c/S that increases with S. The fraction of unpaired spins in $S = 3/2$ junctions is 0.293 for $N = 245$ and 0.302 for $N = 448$; the fraction for $S = 2$ spins is 0.326 for $N = 445$ and 0.323 for $N = 448$. By contrast, the fraction is less than 0.1 in $S = 1$ junctions for $N = 202$ or 199 and clearly vanishes in the infinite junction since unpaired spins are in localized states. The fraction of unpaired spins also goes to zero in $S = 1/2$ junctions with increasing N as discussed earlier.

We generalize Eq. 8 for ρ_r to reflect the different behavior of spin densities near the junction and ends of arms. We study positive and negative ρ_r separately but use the same length for simplicity, ξ for arms and ξ_J for the junction. The spin densities in one arm run from $r = 1$ to n, with $N = 3n+1$ and the junction at $r = n+1$. For even N (odd n), we analyze the spin densities according to

$$\rho_{2r-1} = c + aexp(-(2r-1)/\xi) + a_Jexp(-(n+2-2r)/\xi_J)$$
$$\rho_{2r} = -(c + bexp(-2r/\xi) + b_Jexp(-(n+1-2r)/\xi_J)). \quad (9)$$

The first sum over odd sites has $r = 1, 2, .., (n+1)/2$; the second sum runs to $(n-1)/2$ since there is one fewer even site. Both positive and negative spin densities for odd N (even n) have r up to $n/2$ in Eq. 9.

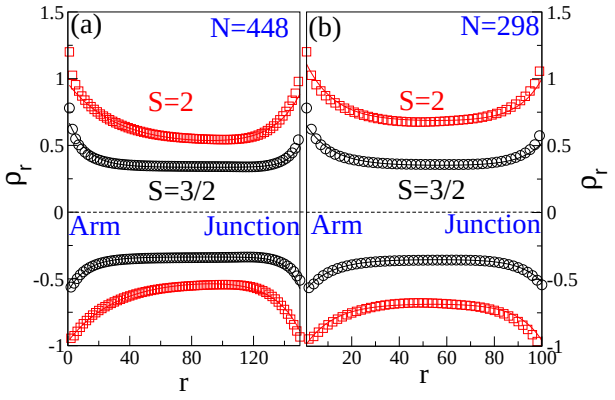

FIG. 8. Spin densities ρ_r in one arm of Y junctions with (a) $N = 448$ and (b) $N = 298$ spins $S = 3/2$ and 2. Lines are Eq. 9 with parameters in Table III

Exponential contributions are limited to either end when $n > \xi$ or ξ_J. The parameters are obtained as shown in Fig. 9 for $N = 448$ ($n = 149$) and $S = 3/2$. The SDW amplitude is $c = 0.336$, ξ_J is significantly smaller than ξ and $\pm\rho_r$ lead to nearly equal ξ or ξ_J. The junction has $\rho_J = -0.510$ for $N = 448$ and 0.480 for $N = 445$; the arms have equal spin densities within a percent or two. The $N = 445$ junction has essentially the same parameters in Eq. 9. Nevertheless, we have $S_G = 3$ for $N = 448$, $S_G = 3/2$ for $N = 445$. The difference is largely due to the junction and its first few neighbors. Both Y junctions with even or odd N support a SDW with equal $\rho_1 > 0$ at the end of all three arms. Figure 10 shows exponential contributions for $S = 2$ junctions with $N = 448$ and $S_G = 4$. Since the slow decrease of spin densities in Fig. 8 and the resulting $\xi \sim 32$ are in the expected range for $\Delta(2) \sim \Delta(1)/5$, the SDW amplitude of $S = 2$ junctions may not be entirely due to end effects. We leave open the behavior of much longer junctions.

Table IV lists the parameters of Eq. 9 for junctions with even N that generate the lines in Fig. 8; essentially the same parameters hold for $N \pm 1$. The size dependence of the $S = 3/2$ junction has apparently saturated or almost saturated at $N \sim 450$, but has not saturated for the $S = 2$ junction. We always find $\xi_J < \xi$, faster decrease of the SDW amplitude near the junction.

The VBS picture has localized $S = 1$ states at ends of $S = 2$ chains or the arms in $S = 2$ junctions. We find decreasing $\rho_1 = 1.202$ and 1.200 for $N = 298$ and 448 junctions while Schollwöck *et al.* [30] report 1.13 for a chain $N = 270$ with a fixed $S = 1$ defect at the other end. The next site has $\rho_2 \sim -0.95$. The first $5 - 10$ spin densities deviate significantly from Eq. 8, and we

TABLE IV. Eq. 9 parameters for Y junctions of N sites with spin S

S, N	c	ξ	ξ_J	a, a_J	b, b_J
3/2, 148	0.433	5.2	5.7	0.38, 0.25	0.24, 0.20
3/2, 298	0.350	11.2	9.1	0.30, 0.21	0.24, 0.19
3/2, 448	0.336	12.2	7.9	0.33, 0.22	0.26, 0.27
2, 298	0.68	12	10	0.43, 0.39	0.33, 0.34
2, 448	0.54	32	20	0.58, 0.50	0.52, 0.47

do not know how to identify a localized state. The $S = 3/2$ junction for $N = 298$ and 448 has decreasing $\rho_1 = 0.781$ and 0.780 that, perhaps coincidentally, is again slightly larger than $S/2 = 0.75$. Since the SDW amplitude is S in Néel state $|AF\rangle$, quantum fluctuations reduce AF order by 50% at the ends of arms and by more than 50% elsewhere. SDWs occur naturally in systems whose GS has $S_G > 0$ and $2S_G+1$ degeneracy in S_z.

To conclude this Subsection, we comment on $S = 3/2$ and 2 chains with open boundary conditions that were motivated (i) by the unexpected result that $S = 2$ junctions do not follow VBS and (ii) to confirm quantitative agreement with Schollwöck *et al.* [30]. The GS of quantum chains with an even number of spins N is a singlet, $S_G = 0$. It is not degenerate, thereby excluding a SDW, but may have quasi-long-range order in the infinite chain. Delocalized states are expected in the gapless $S = 3/2$ chain. The gapped $S = 2$ chain may have localized $S = 1$ states at either end that become decoupled in the infinite chain. Two localized states lead to exponentially small gaps between the singlet GS, a triplet and a quintet, just as $S = 1$ chains have an exponentially small gap to the lowest triplet [33]. Accordingly, we studied the quintet, $S_G = 2$, with the lowest energy of $S = 2$ chains and for compar-

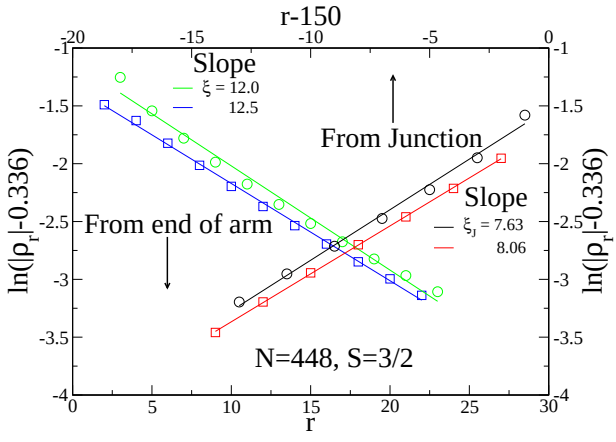

FIG. 9. Spin densities from Fig. 8 for $S = 3/2$, $N = 448$ plotted as $ln(|\rho_r| - 0.336)$ vs. r at an arm and at the junction.

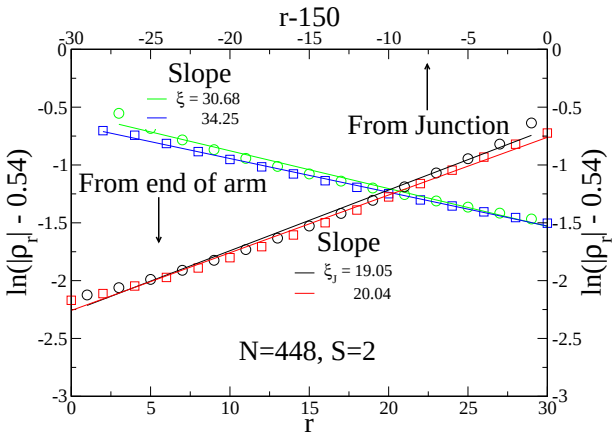

FIG. 10. Spin densities from Fig. 8 for $S = 2$, $N = 448$ plotted as $ln(|\rho_r| - 0.54)$ vs. r at an arm and at the junction.

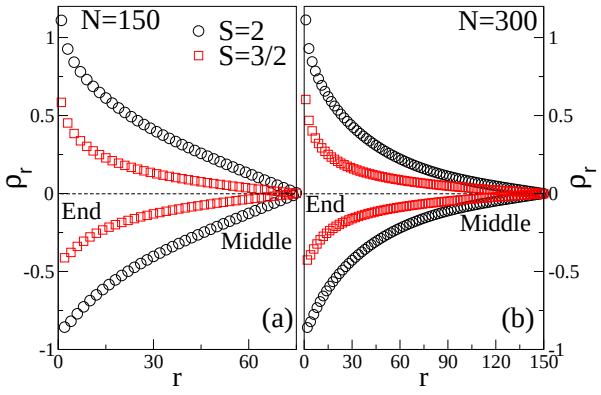

FIG. 11. Spin densities ρ_r in half chains of (a) $N = 150$ and (b) $N = 300$ spins $S = 3/2$ and 2 with antiferromagnetic Heisenberg exchange J between neighbors

ison the lowest-energy triplet, $S_G = 1$, of $S = 3/2$ chains.

Spin densities for open $S = 3/2$ and 2 chains of $N = 150$ and 300 spins are shown in Fig. 11 up to the middle, where they are zero by symmetry. In either case, the first few ρ_r depend weakly on size, as found previously [30], and are almost the same as in $N = 450$ junctions with 150-site arms. End effects are similar in chains and junctions, and exponential fits over a limited range are possible aside from the first few spin densities. Symmetry about the middle of chains leads to linear ρ_r around $r = N/2$ as shown in Fig. 11. The fraction of unpaired spins is large: 0.183 and 0.121 for $S = 2$, $N = 150$ and 300; 0.090 and 0.067 for $S = 3/2$, $N = 150$ and 300. We infer that the spin densities are primarily due to end effects in these chains or junctions, in sharp contrast to the localized states in $S = 1$ chains or junctions.

IV. DISCUSSION

We have presented a modified DMRG algorithm for Y junctions in Section II and results in Section III for junctions up to 500 sites, mainly junctions in Eq. 1 with Heisenberg exchange J between spins $S = 1/2$, 1, 3/2 or 2. Much longer chains of, say, 1000 sites greatly increase the computational effort at the finite DMRG step. The accuracy may not be lower, however, since the entanglement entropy [28] of the GS for dividing the junction into system and environmental blocks will increase only slightly. As already noted, we are considering large but finite junctions rather than the thermodynamic limit. That limit is better studied in chains since neither the junction nor the ends of arms should matter in junctions with infinitely long arms.

The accuracy of the modified algorithm is fully equal to the DMRG accuracy for 1D chains. Two arms are never combined into one and new sites are always bonded to the most recently added sites. As in chains, the superblock Hamiltonian contains only new or once renormalized operators. Infinite DMRG is accurate for $S = 1/2$ or 1 junctions, where finite DMRG makes minimal improvements, but finite DMRG significantly improves the results for $S = 3/2$ or 2 junctions. Three or four sweeps of finite DMRG is sufficient for good energy convergence. We performed $5 - 10$ sweeps for spin densities in order to confirm the different GS of $S = 1$ and 2 junctions.

The modified algorithm for Y junctions of equal arms can be generalized to other systems, to be discussed elsewhere [35]. All generalizations are based on the schematic procedures in Figs. 2 and 3 for equal arms. (i) No change is required for more than three equal arms, although computational requirement increase as discussed on Section II on going from chains to three arms. (ii) The algorithm performs well in preliminary tests of Y junctions with arms of different lengths $n \neq n' \neq n''$ [35]. The infinite algorithm with equal arms is run until the longest arm n is reached. Finite DMRG is then done using blocks of different size to construct the superblock. (iii) GW considered Y junctions with arms that meet at an equilateral triangle instead of a point [17]. For such systems, the modified infinite algorithm can again be used to generate the desired junction. In the beginning of finite DMRG, the superblock is constructed using blocks of different size; [35] two blocks have the same size, the third block has one fewer site, and the new site is added to the third block. The modified algorithm can also be generalized to (iv) Y junctions with different S;

we use four new sites with different S and three arms at every step [35]. A new site is added at the end of each arm and another one is added at the junction of these three arms in Fig. 2. Since the size of the density matrix is $L = (2S+1)^2 m^2$ for adding one spin S, the size scales as $(2S+1)^8$ for adding four spins S. The procedure is efficient for small S but rapidly becomes more expensive for large S.

Kekulé diagrams are special cases of VB diagrams in which singlet pairing is limited to adjacent atoms or to adjacent $S = 1/2$ sites. The complete VB basis also has singlet pairing of more distant sites. There are N_A Kekulé diagrams for the $S = 1/2$ junction with odd N: the unpaired electron is at a site of the larger sublattice, which uniquely fixes singlet pairing, shown as lines to neighbors, of all remaining sites. Although the total number of VB diagrams is exponentially larger, Kekulé diagrams are often a simple approximation for fermionic or spin-1/2 systems that provides semi-quantitative information; they have been extensively used in organic chemistry for well over a century. Their scope now extends to VBS in which $S \geq 1$ sites are represented [22, 30, 34] as two or more $S = 1/2$ spins that are singlet paired with neighbors. VBS has $2S$ lines to neighbors and no unpaired spins aside from chain ends. Unpaired spins and resonance among Kekulé diagrams account naturally for localized $S_z = 1/2$ state in $S = 1$ junctions, albeit without any reference to the Haldane gap.

VBS wave functions are exact GS of special Hamiltonians that Schollwöck *et al.* [30] discuss and write explicitly for $S = 2$ chains. Heisenberg chains with finite $\Delta(S)$ for integer S have bilinear exchange $JS_r \cdot S_{r+1}$ between neighbors while H_{VBS} contains terms up to $(S_r \cdot S_{r+1})^4$ for $S = 2$. Schollwöck and Jolicoeur [32] find that the Haldane phase described by VBS is strongly reduced in $S = 2$ chains compared to $S = 1$ chains. Our DMRG results for finite Y junctions are quite consistent with VBS for $S = 1$ junctions where quantum fluctuations suppress AF order. DMRG for $S = 2$ junctions does not follow VBS, however. The GS is instead a SDW with reduced but finite AF order.

Acknowledgements MK thanks DST for a Ramanujan Fellowship SR/S2/RJN-69/2012 and DST for funding computation facility through SNB/MK/14-15/137. ZGS thanks NSF for partial support of this work through the Princeton MRSEC (DMR-0819860). SR thanks DST India for financial support.

[1] J. Huang, F. Pierre, T.T. Heikkila, F.K. Wilhelm, and N.O. Birge, Phys. Rev. B **66**, 020507 (2002).

[2] C. Papadopoulos, A. Rakitin, J. Li, A.S. Vedeneev and J.M. Xu, Phys. Rev. Lett. **85**, 3476 (2000).

[3] F. L. Deepak, N. Susan John, A. Govindaraj, G.U. Kulkarni and C.N.R. Rao, Chem. Phys. Lett. **411**, 468 (2005).

[4] P. R. Bandaru, C. Daraio, S. Jin and A.M. Rao, Nature Materials **4**, 663 (2005).

[5] S. Das and S. Rao, Phys. Rev B **78**, 205421 (2008).

[6] C. Wang and D. E. Feldman, Phys. Rev. B **83**, 045302 (2011).

[7] C. Y. Hou and C. Chamon, Phys. Rev. B **77**, 155422 (2008).

[8] A. Rahmani, C. Y Hou, A. Feiguin, C. Chamon, and I. Affleck, Phys. Rev. Lett. **105**, 226803 (2010).

[9] D.N. Aristov and P. Wölfle, Phys. Rev. B **88**, 075131 (2013).

[10] C. Wang and D.E. Feldman, Phys. Rev. B **83**, 045302 (2011).

[11] A. Soori and D. Sen, EPL, **93** 57007 (2011).

[12] A. Agarwal, S. Das, S. Rao and D. Sen, Phys. Rev. Lett. **103**, 026401 (2009).

[13] C. Chamon, M. Oshikawa and I. Affleck, Phys. Rev. Lett. **91**, 206403 (2003).

[14] A. Tokuno, M. Oshikawa and E. Demler, Phys. Rev. Lett **100**, 140402 (2008).

[15] D. Giuliano and P. Sodano, Nuclear Phys. B, **811**, 395 (2009).

[16] S. R. White, Phys. Rev. Lett. **69**, 2863 (1992).

[17] H. Guo and S. R. White, Phys. Rev. B **74**, 060401 (R) (2006).

[18] Y. -Y. Shi, L. -M. Duan and G. Vidal, Phys. Rev. A **74**, 022320 (2006).

[19] N. Nakatani and G. K-L. Chan, J. Chem. Phys. **138**, 134113 (2013).

[20] P. Dowd, Accounts Chem. Res. **5**, 242 (1971).

[21] Y. Teki and K. Itoh, in Magnetic Properties of Organic Materials, P.M. Lahti, Ed. (Marcel Decker, New York, 1999), Ch. 12, p. 237.

[22] I. Affleck, T. Kennedy, E.H. Lieb and H. Tasaki, Cummun. Math. Phys. **115**, 4777 (1988).

[23] S. R. White and D.A. Huse, Phys. Rev. B **48**, 3844 (1993).

[24] U. Schollwöck, Rev. Mod. Phys. **77**, 259 (2005).

[25] K. Hallberg, Adv. Phys. **55**, 477 (2006).

[26] M. Kumar, S. Ramasesha and Z.G. Soos, Phys. Rev. B **85**, 134415 (2012).

[27] M. Kumar, Z.G. Soos, D. Sen and S. Ramasesha, Phys. Rev. B **81**, 104406 (2010).

[28] S. Sahoo, V M L Durga Prasad Goli, S. Ramasesha and D. Sen, J. Phys.: Condens. Matter **24**, 115601 (2012).

[29] F. D. M. Haldane, Phys. Rev. Lett. **50**, 1153 (1983); Phys. Lett. A **93**, 464 (1983).

[30] U. Schollwöck, O. Golinelli and T. Jolicoeur, Phys. Rev. B **54**, 4038 (1996).

[31] H. Nakano and A. Terai, J. Phys. Soc. Jpn. **78**, 014003 (2009).

[32] U. Schollwöck and T. Jolicoeur, EPL **30**, 493 (1995).

[33] S. R. White, Phys. Rev. B **48**, 10345 (1993).

[34] A. Kitazawa and K. Nomura, J. Phys. Soc. Jpn. **66**, 3379 (1997).

[35] A. Parvej *et al.* (unpublished).